Proceedings of the 14th Asian Control Conference
July 5-8, 2024, Dalian, China

An Authority Allocation Strategy for Shared Control in Human-Machine Cooperative Driving via Lane-Based Probabilistic Collision Risk Assessment

Xiuhua Liang[1], Yunbo Zhao[1,2,3], Yu Kang*[1,2,3,4], Chang Xu[1]

***Abstract*—An effective shared control strategy plays a crucial role in assisting drivers during hazardous situations in human-machine cooperative driving. This study introduces an authority allocation strategy for shared control based on collision risk assessment in a long-term maneuver. Initially, maneuvers are categorized by lanes, which can properly represent lane-based driving characteristics in real-world driving conditions. Subsequently, multiple lane models are built to combine with interactive multiple models to compute target lane probabilities. The target lane probabilities indicate the likelihood of a vehicle moving toward or remaining in each lane, determined by its lateral position in curvilinear coordinates. Finally, collision risk is evaluated through the integration of model probability distribution of lanes and artificial potential field value between a pair of predicted trajectories. Intuitively, the driver's authority is directly correlated with the collision risk, so authorities between the driver and the machine are determined by the collision risk through a piecewise proportional function. The effectiveness of the proposed algorithm is verified using the Carla simulator in a cut-in scenario.**

***Index Terms*—Risk assessment, Artificial Potential Field, Authority Allocation Strategy, Shared Control**

I. Introduction

Constrained by technical bottlenecks and ethical dilemmas, autonomous driving in arbitrarily open, complex, and unstructured environment is deemed as an unattainable goal in the foreseeable future [1] [2]. To address this, driver-machine cooperation, leveraging the strengths of both entities, offers a viable solution. Shared control, as a primary form of human-machine cooperative driving, entails simultaneous involvement of the driver and the machine in controlling vehicle [3].

Research in shared control primarily focuses on devising strategies that allocate the driving authorities between the driver and the machine under ever-changing driving circumstances. Some studies opt to design strategies based on the monitored state of the driver (e.g., fatigue and distraction levels), despite the tenuous link between the driver's status and driving performance efficiency [4].

Another category of authority allocation strategy involves evaluating collision risk between the ego vehicle and surrounding vehicles. Various studies adopt Artificial Potential Field(APF) [5] [6] and Time-To-X (TTX) metrics, such as Time-To-Collision (TTC), Time-To-React (TTR) or Time-To-Steer (TTS) [7] [8] to assess collision risk and determine authority allocation strategy. However, above deterministic approaches which employ simplified future prediction models like Constant Yaw Rate and Acceleration (CYRA), are only used effectively in a short time and have not enough foresight to handle uncertainty in long-term motion prediction due to their simplistic nature. To model uncertainty in long-term motion prediction, methods focusing on maneuver-based trajectory prediction are proposed, since the evolution over a long time is much stronger influenced by the intentions, motivations, and goals of all traffic participants. These approaches categorize driving behaviors into different maneuvers and then generate trajectories aligned with corresponding identified maneuvers based on reasonable assumptions. Although there are attempts to model the uncertainty based on Gaussian distribution through random sampling [9], these methods overlook critical factors such as road geometry and lane-based driving characteristics, and thus cannot properly represent the motion uncertainties in real-world driving conditions.

Therefore, in this study, we propose multiple lane models which consider factors like road geometry, constraints in vehicle dynamics and lane-based driving characteristics in collision risk assessment during a long-term maneuver. More specifically, multiple lane models are based on lane-based maneuver where the vehicle gradually approaches the centerline of the target lane with small variation, as excessive lateral velocity can cause the vehicle to roll over. In contrast with the existing collision risk assessment established upon current situation or linear assumption of future trajectories, the future motion uncertainty over a longer time horizon is modeled with respect to long-term lane-based maneuvers and the corresponding probability distribution. Using multiple lane models, lane-based probabilistic maneuver prediction of surrounding vehicles and ego vehicle are computed by Interactive Multiple Models (IMM), followed by trajectory generation of each vehicle using quintic polynomial. Finally, the collision risk is assessed by the use of both an Artificial Potential Field (APF) value between two trajectories (ego and surrounding

*Corresponding author. E-mail: kangduyu@ustc.edu.cn
This work was supported by the Dreams Foundation of Jianghuai Advance Technology Center (NO.Q/JH-063-2023-T02 A/O)
[1]Department of Automation, University of Science and Technology of China, Hefei, China
[2]Institute of Artificial Intelligence, Hefei Comprehensive National Science Center, Hefei, China
[3]Institute of Advanced Technology, University of Science and Technology of China, Hefei, China
[4]Anhui Province Key Laboratory of Intelligent Low-Carbon Information Technology and Equipment, University of Science and Technology of China, Hefei, China

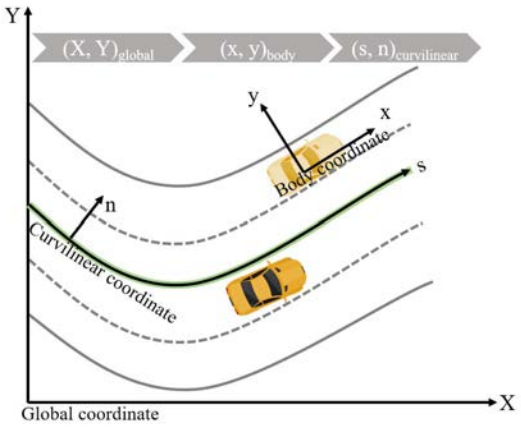

Fig. 1: The diagram of three coordinates.

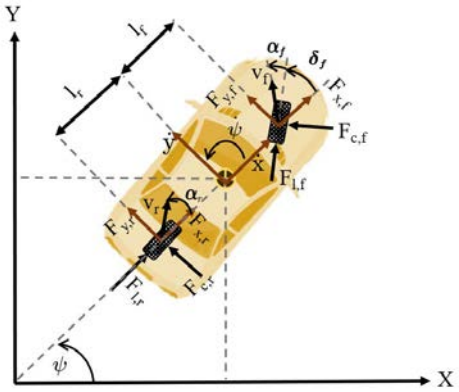

Fig. 2: The diagram of vehicle dynamics.

vehicle trajectories) and the probability distribution of lane model.

This paper is structured as follows. Section II introduces curvilinear coordinates to describe road geometry and vehicle dynamics. Section III models the lane-based maneuvers and gives a trajectory generation method. Section IV details the authority allocation strategy based on collision risk and involves directly combining commands from the driver and the machine based on their respective levels of authority in shared control. Section V presents a simulation of a cut-in scenario to demonstrate the effectiveness of the proposed method.

II. Preliminary

A. Curvilinear Coordinates

The trajectories in this study are analyzed based on curvilinear coordinates, which are better suited for describing vehicle positions on roads with varying curvatures. The curvilinear coordinates are established in accordance with the road geometry. As Fig. 1 shows, the generation of trajectories is related to the conversion between three types of coordinate systems, global cartesian coordinate (X, Y), curvilinear coordinate (s, n), and vehicle body cartesian coordinate systems (x, y). In the curvilinear coordinate, this reference curve is regarded as $s\text{-}axis$, and the lateral offset from the reference curve is regarded as $n\text{-}axis$.

B. Vehicle Dynamics

Inspired by [10], we use a nonlinear bicycle model to describe the dynamics of vehicle. As Fig. 2 shows, applying Newtons Second Law to longitudinal, lateral, and yaw degrees of freedom, the following set of differential equations are given in

$$\begin{aligned} m\ddot{x} &= m\dot{\psi}\dot{y} + 2\left(F_{x,f} + F_{x,r}\right), \\ m\ddot{y} &= -m\dot{\psi}\dot{x} + 2\left(F_{y,f} + F_{y,r}\right), \\ I_z\ddot{\psi} &= 2\left(l_f F_{y,f} - l_r F_{y,r}\right), \end{aligned} \tag{1}$$

where the states $\dot{x}$,$\dot{y}$ and $\dot{\psi}$ denote the longitudinal and lateral velocity of vehicle body axes and the angular velocity about z-axis. The parameters of the vehicle model are mass m,moment of inertia l_z and distances from the centre of gravity to front and rear axles, denoted as l_f and l_r, respectively. The tyre forces acting on the vehicle body axes are denoted as $F_{i,j}$, where the first subscript $i \in \{x, y\}$ describes the vehicle body axes (i.e. longitudinal, lateral) and the second subscript $j \in \{f, r\}$ describes the tyre (i.e. front and rear). Using δ_f denotes the steering angle of the front tyres, then we can derive

$$\begin{aligned} F_{y,f} &= F_{1,f}\sin(\delta_f) + F_{c,f}\cos(\delta_f), \quad F_{y,r} = F_{c,r}, \\ F_{x,f} &= F_{l,f}\cos(\delta_f) - F_{c,f}\sin(\delta_f), \quad F_{x,r} = F_{l,r}, \end{aligned} \tag{2}$$

where the tyre forces acting on tyre axes are denoted as $F_{i',j'}$. The first subscript $i' \in \{l, c\}$ describes the tyre axes (i.e. longitudinal, lateral) and the second subscript $j' \in \{f, r\}$ describes the tyre (i.e. front and rear). We define the following lateral tyre forces which are proportional to the slip angles in the linear region as

$$F_{c,j'} = -C_{\alpha_{j'}}\alpha_{j'}, \quad j' \in \{f, r\}, \tag{3}$$

where C_{α_f} and C_{α_r} denote the cornering stiffnesses of the front and rear tyres, respectively. And approximating the slip angles as

$$\alpha_f = \frac{\dot{y} + l_f\dot{\psi}}{\dot{x}} - \delta_f, \quad \alpha_r = \frac{\dot{y} - l_r\dot{\psi}}{\dot{x}}. \tag{4}$$

We consider a front steerable vehicle and can derive as

$$F_{l,f} = \frac{1}{2}ma_x, \quad F_{l,r} = 0, \tag{5}$$

where a_x denotes acceleration command generated by throttle and brake.

The conversion from (x, y) to (X, Y) is described by

$$\begin{aligned} \dot{X} &= \dot{x}\cos\psi - \dot{y}\sin\psi, \\ \dot{Y} &= \dot{x}\sin\psi + \dot{y}\cos\psi. \end{aligned} \tag{6}$$

We augment and discretize (1)-(6) by using a forward difference method at a fixed sampling time, which is compactly written as

$$\chi(k+1) = f(\chi(k), u(k)), \tag{7}$$

where $\chi = [\dot{x}, \dot{y}, \psi, \dot{\psi}, X, Y]$, and $u = [a_x, \delta_f]$.

III. Lane-based Trajectory Prediction

In this section, the uncertain future maneuvers of the ego vehicle and surrounding vehicles are modeled by using the Interacting Multiple Models (IMM) framework, a probabilistic model for estimating a multi-modal behavior of vehicles [11] [12]. Compared to cartesian coordinates, the proposed method formulates vehicle trajectories in curvilinear coordinates, which is more appropriate for handling road geometry and constraints.

A. Maneuver Recognition Based on IMM

We divide maneuvers into lane keeping, lane change, lane double change, and so on according to the number of lanes. The details on maneuver recognition based on IMM are as follows.

Assuming $T_{ij} = P(L_{k+1}^j | L_k^i)$ denotes the transition probability which represents the probability of the transition from lane i in prediction time k to lane j in prediction time $k+1$.

1) Interacting(Mixing): In mixing phase, the mixed lateral offset $n_{k+1|k}^{*j}$ and covariance $\Sigma_{k+1|k}^{*j}$ are computed by mixing lane model n_k^i and their respective fusion coefficients $\mu_k^{i|j}$

$$n_{k+1|k}^{*j} = \sum_i n_k^i \cdot \mu_{k+1|k}^{i|j}, \tag{8}$$

$$\Sigma_{k+1|k}^{*j} = \sum_i \mu_{k+1|k}^{i|j} \left(\Sigma_k^i + \left(n_k^i - n_k^{*j} \right) \left(n_k^i - n_k^{*j} \right)^T \right), \tag{9}$$

where

$$\hat{\mu}_{k+1|k}^j = \sum_i T_{ij} \cdot \mu_k^i, \tag{10}$$

and

$$\mu_{k+1|k}^{i|j} = \frac{T_{ij} \cdot \mu_k^i}{\hat{\mu}_{k+1|k}^j}. \tag{11}$$

2) Prediction Model: To describe the nature that the vehicle gradually approaches the centerline of lanes, meanwhile the lateral velocity cannot be too large due to constraints in vehicle dynamics, the lateral offset of the vehicle n along the road is modeled by an intuitively parameterizable, continuous-time Ornstein-Uhlenbeck process [13] described by the following differential equation

$$\Delta \dot{n}^i = -\beta \Delta n^i + w_n, \quad \beta > 0, \tag{12}$$

where $\Delta n^i = n^i - \bar{n}^i$ represents the relative vehicle's lateral offset to target position $\bar{n}^i$ for lane i, as shown in Fig. 3, $\bar{n}^i \sim N(\bar{n}_l, \sigma_w^2)$ denotes Gaussian distribution with respect to the lateral offset of target lane centerline $\bar{n}_l$ in curvilinear coordinates. $w_n \sim N\left(0, \sigma_w^2\right)$, where σ_w^2 is set as $(W_L/4)^2$ to cover deviation from the center of the lane by two-sigma variance, which represents the uncertainty in road geometry. Here, W_L is the width of each lane, and maneuver time constant $T_c = 1/\beta$. Since T_c is uncertain in different maneuvers, so each lane-based maneuver is actually composed of a set of trajectories shown in Fig. 3. The process (12) is discretized via zero-order holdere, the final multiple lane models are written in

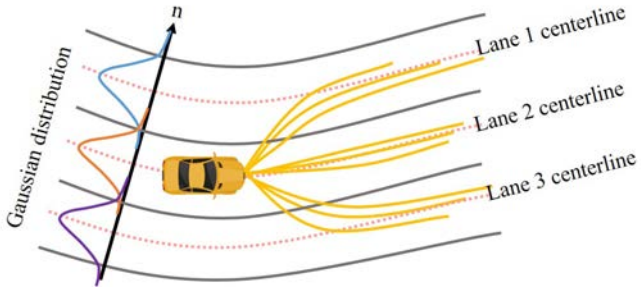

Fig. 3: Multiple lane models with respect to the lateral offsets in curvilinear coordinates for the case of three lanes on the road.

$$n_{k+1}^i - \bar{n}_k^i = e^{-\beta t}(n_k^i - \bar{n}_k^i) + (1 - e^{-\beta t}) w_n, \ \forall \ i \ \in \ (1, 2..., N_l), \tag{13}$$

where t denotes prediction time, N_l is the number of lanes.

3) Model Probability Update: After the prediction step, each lane model probability is updated based on the residual term $\tilde{z}_{k+1}^i$ and its covariance S_{k+1}^i at time $k+1$

$$\tilde{z}_{k+1}^i = z_{k+1} - n_{k+1}^i, \tag{14}$$

$$S_{k+1}^i = P_{k+1}^i + N_{k+1}^i, \tag{15}$$

where $R \sim N(0, \sigma_q^2)$ is the zero-mean white Gaussian measurement noise. The likelihood function of the observation L_k is assumed to be a Gaussian probability density function (PDF) as shown in

$$L_{k+1}^i = \frac{\exp\left[-\frac{1}{2} \left(\tilde{z}_{k+1}^i \right)^T \left(S_{k+1}^i \right)^{-1} \tilde{z}_{k+1}^i \right]}{\sqrt{(2\pi)^{\dim(z)} \left| S_{k+1}^i \right|}}. \tag{16}$$

Then we can get the model probability for each model

$$\mu_{k+1}^i = \frac{\hat{\mu}_{k+1|k}^i L_{k+1}^i}{\sum_j \hat{\mu}_{k+1|k}^j L_{k+1}^j}. \tag{17}$$

B. Trajectory Prediction Based on Quintic Polynomial

After calculating the model probability distribution of lanes, future trajectories of the ego vehicle and surrounding vehicles are generated towards the centerline of each lane. Based on the minimum jerk principle to guarantee comfortable motion [14], trajectories shown in Fig. 4 are generated by using a quintic polynomial as a basis function in the curvilinear coordinates as

$$n = f(s) = a_0 + a_1 s + a_2 s^2 + a_3 s^3 + a_4 s^4 + a_5 s^5, \tag{18}$$

where a_i, $i = 1, 2, ..., 5$ are calculated by following conditions

$$\begin{aligned} n(0) &= n_s \quad \frac{dn(0)}{ds} = \dot{n}_s \quad \frac{d^2 n(0)}{ds^2} = \ddot{n}_s, \\ n\left(s_e\right) &= n_e \quad \frac{dn\left(s_e\right)}{ds} = 0 \quad \frac{d^2 n(0)}{ds^2} = 0, \end{aligned} \tag{19}$$

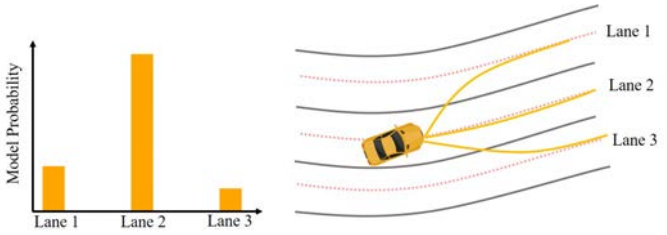

Fig. 4: Trajectory prediction of a vehicle with corresponding model probabilities of road lanes.

Fig. 5: The diagram of a cut-in scenario in Carla simulator where the red car represents the ego vehicle, with a black car on the left lane attempting to cut in due to the slow-moving white car ahead.

where n_s and n_e are the start and end lateral offsets from the road centerline with respect to the arc length s. Here, n_e is the center position of each lane to represent each lane maneuver. $\dot{n}$ and $\ddot{n}$ are the lateral velocity and the lateral acceleration in curvilinear coordinates, respectively. The longitudinal motion is modeled as the constant acceleration model regarding time

$$s_e = v_0 + \frac{1}{2}at^2. \tag{20}$$

IV. SHARED CONTROL

In this section, collision risk of driver's intended maneuver is computed by incorporating artificial potential field (APF) for a pair of generated trajectories and model probabilities of each lane in Section III.

A. Collision Risk Assessment

The repulsive potential $U(x, y)$ between a position (x, y) in the ego vehicle's trajectory and a position (x_s, y_s) in the surrounding vehicle's trajectory at prediction time t is computed by

$$U(x,y) = \exp(-\frac{(x-x_s)^2}{\sigma_x^2} - \frac{(y-y_s)^2}{\sigma_y^2}). \tag{21}$$

The repulsive potential between a driver's intended trajectory Γ_d and a predicted trajectory of an i^{th} surrounding obstacle's trajectory Γ_{s_i} is heuristically summed into a collision risk metric by adding up the repulsive potential of points in Γ_d and Γ_{s_i} at corresponding time t as in

$$R\left(C_{s_i} \mid \Gamma_d, \Gamma_{s_i}\right) = \frac{1}{N_p} \sum_{\substack{(x,y) \in \Gamma_d \\ (x_s,y_s) \in \Gamma_{s_i}}} U\left(x, y\right), \tag{22}$$

where N_p denotes the number of discrete points in a trajectory.

Then, the collision risk of the ego vehicle with an i^{th} surrounding vehicle is computed by considering the model probability of each lane as in

$$R(C_{s_i}) = \sum_{m_k, m_j \in \mathcal{M}} P(m_j)P(m_k)R\left(C_{s_i} \mid \Gamma_d(m_j), \Gamma_{s_i}(m_k)\right), \tag{23}$$

where $P(m_j)$ and $P(m_k)$ are the lane-based maneuver probability distribution of the ego vehicle and the i^{th} surrounding vehicle, respectively. $\mathcal{M}$ is the set of maneuvers. Finally, the collision risk of the driver's intended trajectory for multiple vehicle scenarios can be calculated by

$$R\left(C\right) = \bigcup_{i=1}^{N_s} R\left(C_{s_i}\right) = 1 - \prod_{i=1}^{N_s} \left(1 - R\left(C_{s_i} \mid \Gamma_d\right)\right), \tag{24}$$

where N_s is the number of surrounding vehicles. This value represents the risk possibility that a collision occurs with one of surrounding vehicles when the ego vehicle moves along to driver's intended trajectory.

B. Authority Allocation

Obviously, when collision risk $R\left(C\right)$ increases, driver's authority should decrease for the sake of safety. Therefore, the mapping between the evaluated collision risk and the weight factor of driving authority is established with

$$\lambda = \begin{cases} 1 & R\left(C\right) < R_{th}^L, \\ \kappa R(C) + b & R_{th}^L \leq R\left(C\right) \leq R_{th}^H, \\ 0 & R\left(C\right) > R_{th}^H, \end{cases} \tag{25}$$

where $\kappa = 1/(R_{th}^L - R_{th}^H)$, $b = R_{th}^L/(R_{th}^H - R_{th}^L)$. R_{th}^L and R_{th}^H are the low risk threshold and high risk threshold relating to the driver's style in safety risk, respectively. A higher R_{th}^H and lower R_{th}^L signify more aggressive driver behavior and less willingness to be intervened by the machine.

C. Shared Control

The final input command is a blend of a driver's input and the machine's input directly, denoted as

$$u(k) = \lambda u_d(k) + (1-\lambda)u_m(k), \tag{26}$$

where $u(k)$ refers to the shared steering input which functions as the input of vehicle dynamics in (7). $u_d(k)$ and $u_m(k)$ are the machine's input and the driver's input, respectively.

V. SIMULATIONS

In this section, to verify the effectiveness of the proposed shared control authority allocation strategy, human-machine cooperative driving experiments on a cut-in scenario is conducted using Carla simulator as shown in Fig. 5 where multiple surrounding vehicles are driving on a multi-lane highway road. Parameters of the vehicle dynamics model are presented in Table I.

TABLE I: Vehicle Dynamics Parameters

Parameter	Value
Vehicle mass m (kg)	1720
Length * Width * Height (m)	4.000 * 2.000 * 1.725
Distance from the center of mass to the front axle l_f (m)	1.230
Distance from the center of mass to the rear axis l_r (m)	1.470
Yaw inertia I_z (kg$^2\cdot$ m^2)	4175
Cornering stiffness of front tires $C_{\alpha f}$ (N $\cdot$ rad^{-1})	66900
Cornering stiffness of rear tires $C_{\alpha r}$ (N $\cdot$ rad^{-1})	62700

In order to simulate dangerous driving situations that require human-machine cooperation, the following conditions are considered in the given cut-in scenario as shown in Fig. 5. The ego vehicle is traveling at approximately 24 m/s, the vehicle in the left lane referred to as vehicle 1 cuts in front of the ego vehicle at a distance of 5m at a slightly faster speed due to the slow-moving vehicle ahead referred to as vehicle 2, however, the longitudinal velocity of the vehicle 1 is lower than that of the ego vehicle due to the lane change maneuver, posing a collision risk if the driver of ego vehicle does not take any evasive action. Unfortunately, the driver is distracted by fatigue and fails to notice the cut-in vehicle, continuing to move forward without any brakes.

Fig. 6(a)(b)(c) illustrates lane probabilities of each vehicle computed by IMM method with multiple lane models. It is evident from the figures that both the ego vehicle and vehicle 2 exhibit a high tendency to stay within their respective lanes as shown in Fig. 6(a) and Fig. 6(c), while vehicle 1 starts a lane change around 1.2 seconds, completing the maneuver by approximately 2.8 seconds as shown in Fig. 6(b).

Another shared controller which adopts the APF-based risk assessment strategy based on CYRA assumption of future trajectory is built as a comparison to validate the effectiveness of the proposed lane-based risk assessment strategy. For the sake of clarity in simulation, we refer to our above approach as the Lane-Based APF (LBAPF)-based shared controller. As Fig. 6(f) shown, compared to the driver's constant velocity, LBAPF-based shared controller and APF-based shared controller make a brake and decrease speed to avoid collision. However, the APF-based shared controller exhibits a slower risk perception response compared to the LBAPF-based shared controller as shown in Fig. 6(d), leading to higher risk where the highest risk exceeds 0.2. The delayed risk perception further results in a delayed invention by the machine to correct the driver's wrong behavior as shown in Fig. 6(e).

To further explore the consequences of delayed response, the position distribution of the ego vehicle controlled by the careless driver, APF-based shared controller and LBAPF-based shared controller, along with the probability distribution of lanes for each vehicle, are plotted. Two critical time points, 2.1 seconds and 2.6 seconds, represent the corresponding time points at the highest collision risk point in LBAPF-based shared controller and APF-based shared controller respectively. As Fig. 7(a)(b) shows, at 2.1 seconds, the IMM detects a clear lane change by vehicle 1, but the ego vehicle controlled by APF-based shared controller seems to just realize it, only keeping a little distance away from the cut-in vehicle. As shown in Fig. 7(c)(d), the IMM displays a higher confidence in the lane change behavior of the cut-in vehicle at 2.6 seconds, with the LBAPF-based shared controller already maintaining a safe distance from vehicle 1. Conversely, the APF-based shared controller collides with vehicle 1 by this point. The contrasting outcomes highlight the limitations of the APF-based shared controller in mitigating uncertainties in long-term trajectory prediction, leading to delayed responses and increased collision risk. In contrast, the LBAPF-based shared controller, which integrates future motion uncertainty in the context of road lanes, provides the ego vehicle with sufficient time to react to hazardous scenarios.

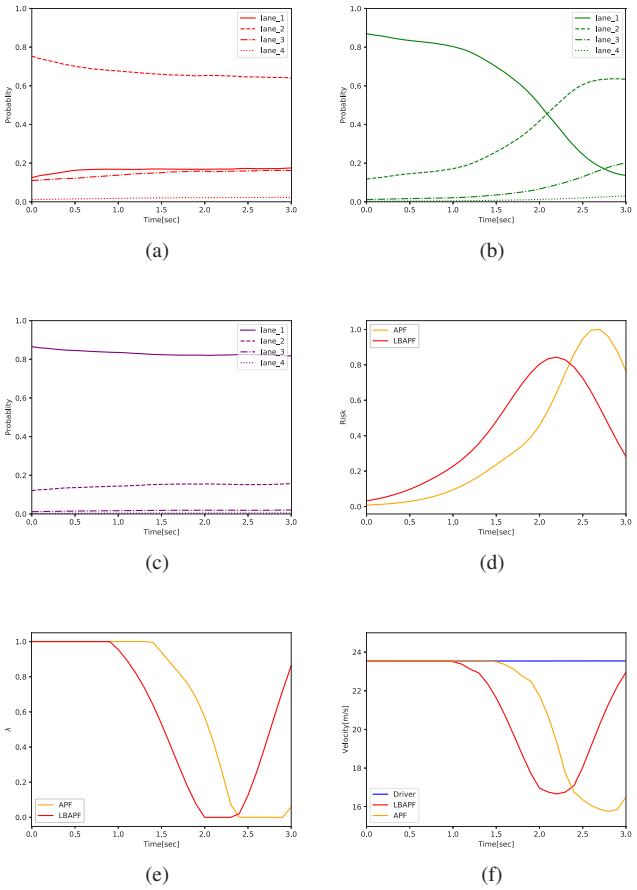

Fig. 6: Figures (a), (b) and (c) represent the target lane probability of ego vehicle controlled by driver, vehicle 1, and vehicle 2 changing over time, respectively. While figures (d), (e) and (f) illustrate risk, allocation authority weight factor, and vehicle velocity changing over time, respectively.

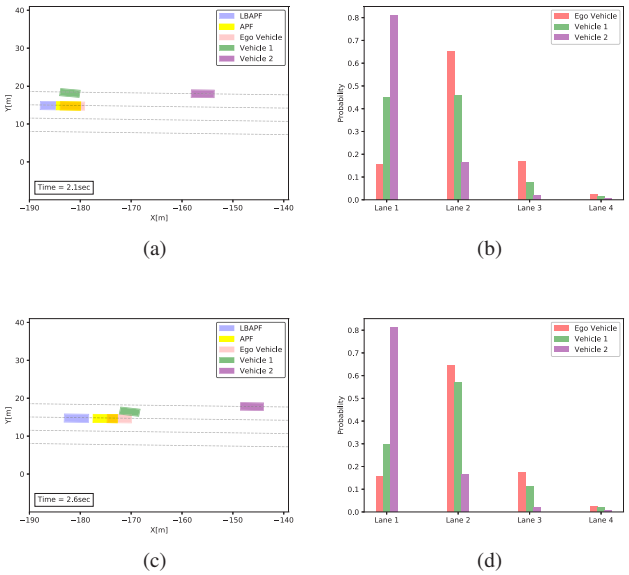

Fig. 7: Figures (a) and (b) illustrate the relative position of the ego vehicle controlled by the driver, APF-based shared controller and lane-based APF shared controller, along with the probability distribution of lanes computed by IMM method for each vehicle at 2.1 seconds. Figures (c) and (d) depict the same information at 2.6 seconds.

VI. Conclusions

In this paper, we introduce a lane-based authority allocation strategy for shared control in human-machine cooperative driving, which is founded on collision risk assessment with surrounding vehicles. The long-term collision risk prediction derives from probabilistic target lane predictions applying the IMM approach, which assists the driver of the ego vehicle by providing sufficient time to react to various complex hazardous scenarios. More specifically, the algorithm incorporates future motion uncertainty within the context of road lanes, allowing for the natural integration of road geometry. It is worth noting that the driver's authority is directly correlated with the collision risk faced by the driver from surrounding vehicles. Consequently, the final authority allocation strategy is determined by the collision risk through the utilization of a piecewise proportional function.

References

[1] J.-F. Bonnefon, A. Shariff, and I. Rahwan, "The social dilemma of autonomous vehicles," *Science*, vol. 352, no. 6293, pp. 1573–1576, June 2016.

[2] S. Ansari, F. Naghdy, and H. Du, "Human-Machine Shared Driving: Challenges and Future Directions," *IEEE Transactions on Intelligent Vehicles*, 2022.

[3] T. B. Sheridan, W. L. Verplank, and T. L. Brooks, "Human/computer control of undersea teleoperators," Nov. 1978.

[4] A. Benloucif, A.-T. Nguyen, C. Sentouh, and J.-C. Popieul, "Cooperative trajectory planning for haptic shared control between driver and automation in highway driving," *IEEE Transactions on Industrial Electronics*, vol. 66, no. 12, pp. 9846–9857, 2019.

[5] H. C. J. W. Y. H. C. H. H. W. Mingjun Li, Xiaolin Song, "Shared control with a novel dynamic authority allocation strategy based on game theory and driving safety field," *Mechanical Systems and Signal Processing*, vol. 124, pp. 199–216, June 2019.

[6] M. Yue, C. Fang, H. Zhang, and J. Shangguan, "Adaptive authority allocation-based driver-automation shared control for autonomous vehicles," *Accident Analysis & Prevention*, vol. 160, p. 106301, Sept. 2021.

[7] M. Li, H. Cao, X. Song, Y. Huang, J. Wang, and Z. Huang, "Shared Control Driver Assistance System Based on Driving Intention and Situation Assessment," *IEEE Transactions on Industrial Informatics*, vol. 14, no. 11, pp. 4982–4994, Nov. 2018.

[8] S. Noh and K. An, "Decision-Making Framework for Automated Driving in Highway Environments," *IEEE Transactions on Intelligent Transportation Systems*, vol. 19, no. 1, pp. 58–71, Jan. 2018.

[9] X. Zhao, Z. Yin, Z. He, L. Nie, K. Li, Y. Kuang, and C. Lei, "Indirect Shared Control Strategy for Human-Machine Cooperative Driving on Hazardous Curvy Roads," *IEEE Transactions on Intelligent Vehicles*, vol. 8, no. 3, pp. 2257–2270, Mar. 2023.

[10] R. Rajamani, *Vehicle Dynamics and Control*. Springer Science & Business Media, Dec. 2011.

[11] R. Toledo-Moreo and M. A. Zamora-Izquierdo, "IMM-Based Lane-Change Prediction in Highways With Low-Cost GPS/INS," *IEEE Transactions on Intelligent Transportation Systems*, vol. 10, no. 1, pp. 180–185, Mar. 2009.

[12] B. Kim, K. Yi, H.-J. Yoo, H.-J. Chong, and B. Ko, "An IMM/EKF Approach for Enhanced Multitarget State Estimation for Application to Integrated Risk Management System," *IEEE Transactions on Vehicular Technology*, vol. 64, no. 3, pp. 876–889, Mar. 2015.

[13] Y. Bar-Shalom, X.-R. Li, and T. Kirubarajan, "Estimation with Applications to Tracking and Navigation: Theory, Algorithms and Software." Wiley, Jan. 2002.

[14] A. Lawitzky, D. Wollherr, and M. Buss, "Maneuver-based risk assessment for high-speed automotive scenarios," in *2012 IEEE/RSJ International Conference on Intelligent Robots and Systems*, Oct. 2012, pp. 1186–1191.